Evidence of critical dynamics in the honey bee swarm

Ivan Shpurov [1,†,‡] (D) ,Tom Froese

[1]   Okinawa Institute of Science and Technology, Embodied Cognitive Science Unit;
[2]   Okinawa Institute of Science and Technology, Embodied Cognitive Science Unit;
[*]   Correspondence: ivan.shpurov@oist.jp;

Abstract: Social insects, such as honey bees exhibit complex behavioral patterns and their inconspicuous coordination enables decision-making on the colony level. It is thus proposed, that a high-level description of their collective behavior might share commonalities with neural processes in the brains. At the same time, recent research concerning overarching features of neural activity implies that brains are poised at the edge of the critical phase transition and that such a state is enabling maximal computational power and adaptability. In our research, we applied some tools developed in the computational neuroscience field to the dataset of bee trajectories recorded within the hive, during the course of many days. Our results imply that certain characteristics of the system are remarkably similar to the Ising model when it operates at critical temperature and also shares some of the features with the human brain at the resting state

1. Introduction

Decision making and cognitive adaptive ability are manifested at different scales of nature. Primates and other mammals are endowed with it, grouping individuals, such as murmurating birds or shoals of fish exhibit it on the collective level, for example by making rapid decisions about the direction of their movement and performing adroit maneuvers to avoid predators. Social insects are capable of creating and supporting sophisticated modes of spatial organization, furthermore they possess the ability for more abstract decision-making. Several lines of research seek to elucidate what traits are shared by entities capable of adaptive behavior, regardless of their mode of operation [1]. A prominent conjecture conceived thought crosspolination of statistical physics and experimental neuroscience is known is the "Critical brain hypothesis". It implies that remarkable adaptive abilities of the neural systems require of them to be poised in the vicinity of critical state. This claim is supported by an enormous trove of experimental data, recorded both *in vitro* and *in vivo*. At the same name, recent research have generated evidence which implies that some collective entites such as as swarms of midges and flocks of birds exhibit hallmarks of the critical state at the collective level. However, a comprehensive assessment of criticality was not done for any of the major types of eusocial insects, such as ants, bees, and termites. Recent advances in the scientific image acquisition and analysis techniques now allow recording trajectories of individual insects [2]. In our work we analyzed a dataset of honey bee trajectories, focusing on the hallmarks of the critical state.

1.1. Smarts in numbers - collective intelligence

Eusocial insects' abilities in foraging [3], enacting complex spatial arrangement of their bodies [4,5] and creating elaborate nesting structures are well-known. Furthermore they could handle making decision on more abstract level. For example, a honeybee colony produces a daughter colony when the original site becomes overcrowded [6]. The choice of nest site depends on a number of parameters and an erroneous decision could lead to the inevitable demise of the colony and all its constituent individuals. Thus, when swarming, bees aggregate themselves into a cluster, usually in a form of penchant hanging from a tree brunch. Then the collective considers information brought by scout bees about the relative

quality of the nearby locations. The swarm evaluates the merits of proposed locations and makes the choice which is then followed thought unanimously, in the overwhelming majority of cases. Everyday functioning of the colony also requires the able handling of incoming information to optimize foraging and allocate tasks for individuals bees.

Ants display similarly complex behavior on the colony level. They are using cooperation to extend their sensing range [7] and engage in complex physical tasks, such as transporting heavy objects or building elaborate structures. Furthermore different colonies demonstrate distinct differences in behavioral patterns across several behavioral traits, thus having a degree of "collective personality", which affects their evolutionary fitness [8].

At a certain level of description mechanism of collective decision-making share common features with such mechanisms within the individual brains [1]. Famous entomologist Thomas D. Seeley [6] noted in his book remarkable similarities between the way in which a honeybee swarm performs the task of making a decision for a new nest site and the activity of a primate brain during a perceptual discrimination task. In both cases, the correct decision is acquired through the non-linear aggregation of activity of individual constituents of the system. Other studies showed [9], that bee colonies adhere to the same psychophysical laws humans do when making decisions while facing varied and conflicting sources of information

A fundamental organizing principle shared by the brain and eusocial insects is that all forms of behavior and cognitive ability arise from the local interactions between the system's elements, be it insects on neurons, and does not need to be explicitly organized with a blueprint or central pacemaker of some sort.

1.2. Critical brain theory

In the neuroscience field, it has been conjectured that healthy brains are poised in the vicinity of second-order phase transition [10–13]. Unlike the more familiar case of first-order transition, exemplified by the freezing of water, the second-order transition does not have a sharp boundary separating the two phases. In the vicinity of the critical point, both states of matter could coexist and the system displays a set of remarkable characteristics: most notably, long-range correlations link distant locations, and events of all scales could occur in the system [14].

Recordings of Local Field potentials (LFPs) from cortical slices [15], as well as an analysis of neural data of different modalities, including EEG, MEG, and fMRI [16,17], showed that both the isolated neural tissue and the intact functioning brains exhibit statistical properties characteristic of the system in the critical state. Most importantly the size of fluctuations in the system scales abides by the power-law scaling, making events of all sizes possible, long-range correlations exist in both temporal and spatial domains, and patterns of dynamic activity exhibited by the system exhibit complexity and variability significantly exceeding what would be expected by random chance. Furthermore, research in the field showed that such a state might be not epiphenomenal (i.e consequent of but nor causal to), but necessary to maintain the brain's functionality [12].

This view, which became known as the "critical brain theory", conjectures that the critical state of the system underlies its key functionality, including its ability to produce a wide range of emergent configurations of activity. Emergent behavior is paramount for an adaptive system, as it underlies its ability to produce multitude of responses without altering the underlying structure.

It has been established that in the vicinity of the critical point the system has the widest repertoire of dynamic patterns emerging from local interactions only [18]. A body of evidence, accumulated through computational models and experiments with cortical slices, shows that at critical state neural networks are best suited for complex computation. Information transmission, integration [19], and representation [20] are optimal dynamic range is maximized [21], allowing the networks to respond to a wide range of stimuli. These findings are corroborated by medical research showing that deviations from criticality are correlated with suboptimal mental states in humans [22].

1.3. Evidence for criticality in collective behavior

Evidence of criticality and its implications discussed above 1.3 applies mostly to mammalian brains. As we argue in 1.1insect communities, despite having a little structural resemblance to the brains share the same burden of navigating the world and making choices crucial to survival.

The universality of physical laws implies that different systems could be described with the same set of basic laws. At the same time principles of convergent evolution make it possible that similar phenomena could come to be in unrelated species if they are advantageous to survival. Given the benefits critical state confers to the adaptive ability of the systems, it is fitting to conjecture that swarms and colonies of collective insects would evolve to be positioned in its vicinity. Investigations of brains' critical phenomena focus on analyzing patterns of electric signals (EEG, LFP, MEG) or alternatively using proxy metrics for brain activity (fMRI). Animal collectives use many modes of interaction to exchange information and synchronize actions within the group, including vocal cues, movements, and phenomenal signals. Previous research we reviewed assumes unanimously, that the spatial and temporal scale at which critical phenomena would presumably be exhibited by such systems, makes the movement patterns, correlations, and derivatives thereof the best venue for analysis.

Recent research showed that critical phenomena are observable in flocking birds [23] and swarming of midges [24,25]. Long-range velocity correlations underlie the astonishing ability of these creatures to maneuver collectively with the synchronicity of one. Cursory evidence exists, to suggest that ants make use of enhanced coordination between individuals conferred by criticality to maximize the load carrying capacity of a group [26] and optimize forage route allocation [27].

2. Materials and Methods

2.1. Bee data

All bee data analyzed in this paper was provided by professor G. Robinson and his team. Their recent paper explains the nuances of the methods [2]. To summarise briefly: five trials were conducted, each using a colony of 1200 worker bees. Insects were marked with barcodes attached to the thorax. Colonies resided in the rectangular hives which had video cameras installed inside. Barcodes enabled tracking the positions of individual insects. Several days and nights of activity were recorded for each colony. For the first two days and two nights of each trial, hives were kept sealed and supplied with the necessary nutrients. Afterward bees were allowed to leave at will to scout and forage.

Raw dataset, contained IDs and coordinates accompanied by UNIX timestamps. We developed a prepossessing pipeline using linear interpolation to re-sample individual trajectories at uniform time intervals. Data was partitioned into day and night intervals. Bees that were inactive were filtered out. During our analysis we focused on the period of time, when bees were sealed inside the hive, assuming that such a condition is similar to the resting state of the brain.

For each insect we compute its Kinetic Energy from the horizontal and vertical displacement over time (1). Such an approach was first implemented [28] to identify bursts of activity in bee hives. It should be noted that the purpose of computing kinetic energy is that it provides a convenient proxy to measure the change in activity over time, thus physically rigorous details, such as accounting for mass of each bee could be omitted. Figure 1 illustrates kinetic energy is computed. To characterize activity of a hive as a whole mean kinetic energy, K_{mean} is computed according to (2)

$$K_{bee}(t) = \Delta x^2 + \Delta y^2 \tag{1}$$

$$K_{mean}(t) = \sum_{i=1}^{n} K_i \tag{2}$$
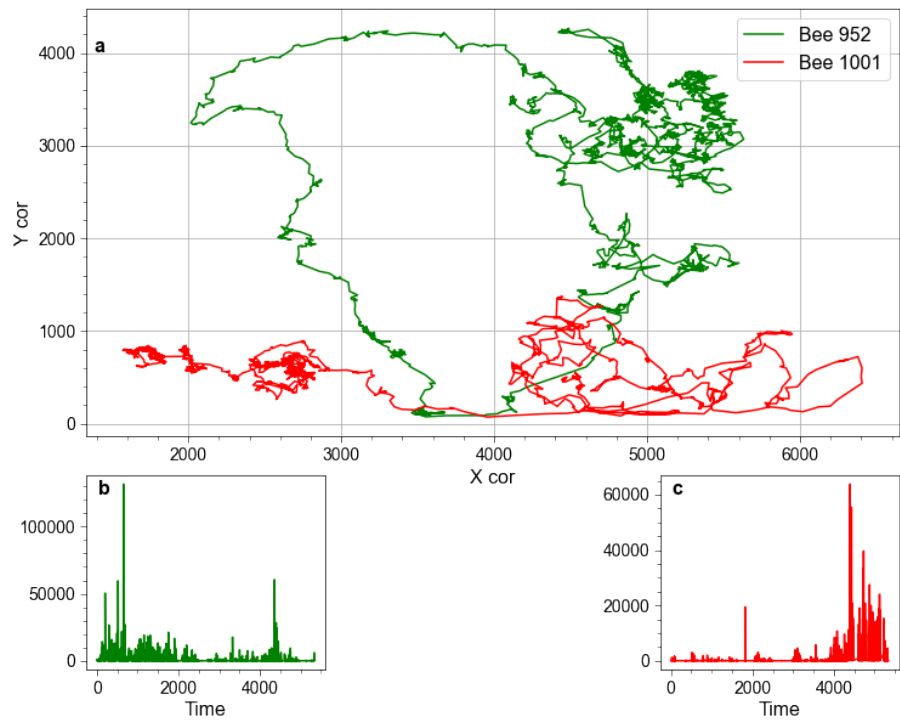
Figure 1. Illustrative example demonstrating how spatial coordinates are converted to kinetic energy. Pane (**a**) presents fragments of trajectories of two bees recorded during the first day of Trial 1. Panes (**b**) and (**c**) respectively show kinetic energy time-series computed from their movements.

2.2. The Ising Model

The Ising model is one of the simplest models which exhibits critical behavior. It consists of a square lattice with sides of length L which is composed of $N = L \times L$ sites with nearest neighbor interactions. Each site has an associated binary "spin" variable $s_i = \pm 1$. Lattice configuration is uniquely specified by a sequence of spin variables. For a system-level description of the model two order parameters - Magnetisation (3), which corresponds to the mean spin of the model, and Energy (4) are computed.

$$M = \frac{1}{N} \sum_{i=1}^{N} s_i \tag{3}$$

$$E = -J \sum_{i,j=nn(i)}^{N} s_i s_j \tag{4}$$

Neighboring spins tend to align with each other, with alignment probability controlled by the temperature parameter T. Competition between thermal fluctuations, which induce chaotic behavior, and the nearest neighbor interactions, which pull the system towards a more ordered state govern the dynamics of the model. At low temperatures $T = T_{low}$ the system soon finds itself in a quiescent state. High temperature $T = T_{high}$ causes uncorrelated, random activity. In the vicinity of the critical point, when $T \approx T_{crit}$ the system exhibits a multitude of critical phenomena, such as long-range temporal and spatial correlations and complex patterns of activity.

We implemented the Metropolis Monte Carlo algorithm [29] to solve for the equilibrium configuration of the model. Details of the algorithm are given in the Appendix A.1.

Each step of the algorithm consists of N site updates. Initially, the system is allowed to settle into an equilibrium state. During this process, known as thermalization no recordings are taken. In our implementation, this stage lasts 10000 steps. Then 2000 consecutive configurations of the model, separated by one step of the algorithm are recorded. We used 3 Ising models of size $N = 10000$ with their T parameter set respectively at $T_{low} = 2.0$, $T_{crit} = 2.3$ and $T_{high} = 3.0$. We considered necessary to use a model of sufficient size to make the statistical tests we perform more scrupulous.

2.3. Dynamic Correlations

Our approach to constructing and analyzing graphs of dynamic correlations was influenced by a seminal paper [16] which used network approach to compare brain dynamics inferred from resting state fMRI recordings with Ising model at different temperatures. Thus, we tried to keep consistency with methods whenever it was possible, given different nature of the data.

To construct correlation networks we treat each site of the Ising model and each bee as node, while edges are inferred from correlations between activity of different nodes (i. e either between Kinetic energy time-series of individual bees, or between the time-series of spins of different lattice sites of the Ising Model). Correlations are computed using Pearson's correlation r coefficient (5) which captures the degree of linear correlation between the two time series. Nodes are connected with edges, when correlation exceeds some predefined threshold p.

$$r(x,y) = \frac{\mathbb{E}[(X - \mu_x)(Y - \mu_y)]}{\sigma(x)\sigma(y)} \tag{5}$$

A meaningful way to compare networks which have very different provenance is to scan a range of p values for each of the networks at hand, while simultaneously computing networks' average degree $\langle k \rangle$. Then, comparisons could be made between networks of similar $\langle k \rangle$. Figure 2 illustrates this approach for Ising networks at 3 different temperatures and for the network derived from the correlations between kinetic energy time-series of bees during 1 day. Exemplifying case of $\langle k \rangle \approx 60$ is used.

After constructing correlation networks for different systems we investigate their degree distributions and other network metrics. Important step is to access if the degree distribution of the system follows the power-law. It has been brought up by the statistical community [30] that often methods used to characterize power-law relationships in statistical research don't stand up to mathematical scrutiny. We used what is considered to be the cutting-edge methods [31] to make our assumptions. Some caveats and supplementary information are contained in the B.2.
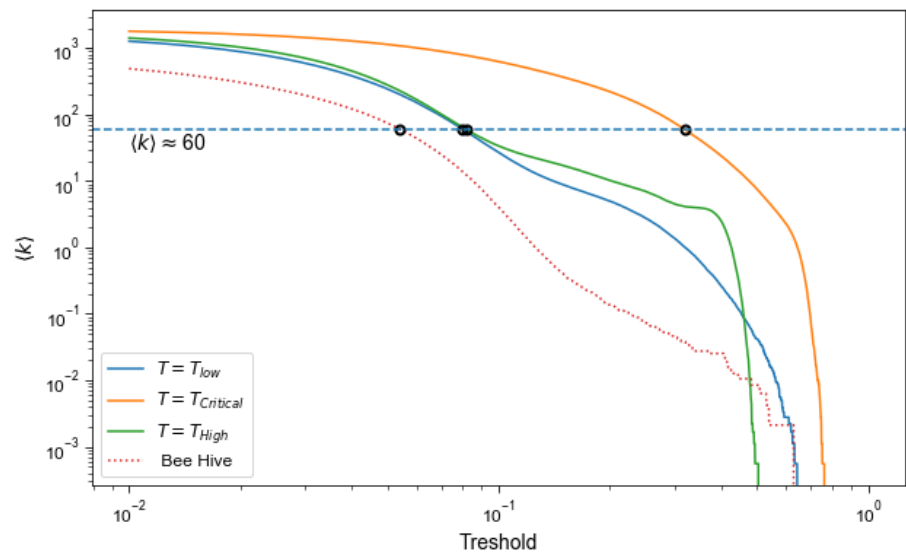
Figure 2. Dependence of the mean degree $\langle k \rangle$ on the threshold p used for binarisation. The dashed line shows a specific degree chosen to compare different networks, black circles indicate resultant relations between $\langle k \rangle$ and p

2.4. Temporal Analysis

Correlations networks analysis elucidates the degree of correlation between time-series of different nodes. However, previous research, concerning both neurological recordings [32] and computational models [33] which are known to exhibit critical behavior showed that such time-series exhibit significant autocorrelations - patterns of activity at one timestep significantly influence activity at the lagged time interval. The established method to quantitatively characterize the degree of autocorelation in the time-series is the Hurst exponent H [34].

It is a scalar metric that ranges between 0 and 1. For random walks and patterns of Brownian motion, in which successive timesteps are completely independent $H \approx$ 0.5. Such processes are called memoryless. Values of H close to one imply significant positive autocorrelations in the data, while values of H between 0 and 0.5 imply negative autocorrelation.

Several approaches to computing H exist all of them having different pros and cons. We adapted simplified methodology initially developed for stock market analysis [35] and rigorously tested our implementation on synthetic data. For a timeseries $S(t)$ we compute cumulative sum of its deviations from the mean (6).

$$S^{sum}(t) = \sum_{1}^{S} S(t) - \mu_s \tag{6}$$

Then we compute variance for a sequence of lags τ.

$$Var(\tau) = \langle |S^{sum}_{t+\tau} - S^{sum}_t|^2 \rangle \tag{7}$$

For Brownian motion variance is linearly dependent on lag $Var(\tau) \propto \tau$. However, when autocorelations are present this relation acquires anomalous exponent $Var(\tau) \propto \tau^H$. We compute H by solving for relation between $log(Var(\tau))$ and $\log(\tau)$.

3. Results

3.1. Model Graphs

Figure 3 depicts degree distributions of correlation networks created using the Ising model at 3 different temperatures as well as an illustrative degree distribution for the correlation network computed using kinetic energy time-series of bees recorded during one day. Earlier [16] work used an analogous approach to compare fMRI correlation network with Ising model at $T = T_{crit}$. It is important to underline, that it is not assumed that either brain or bee hive share structural similarities with the Ising model, most notable difference being that in the Ising model only possesses nearest neighbor interactions, while brains have intricate wiring patterns with long-range connections and bees are able to move freely inside the hive and thus interact with any other individual of their choosing. However, it is possible to use the Ising model as the "worst case" scenario to show that even when the such simplifying assumption is made remarkable similarities are present between the dynamics of the system in question and the known model of the critical state.

Several methods have been used to analyze criticality in neural data. We choose to use the network approach for our initial test for a number of reasons. Firstly, unlike fMRI voxels or neurons, bees could move freely inside the hive. Thus, some methods which rely on measuring spatially localized activity, for example, the local field potentials in different areas of the neural tissue, would be challenging to apply. Using correlations between kinetic energy time-series of individual bees allows to circumvent this difficulty and still have a data which could be directly compatible to the Ising model.

From observing Figure 3 it is evident that the degree distribution of the Ising model at the critical temperature and degree distribution of the bee correlation matrix share a similar long-tailed structure, regardless of the mean degree chosen for comparison, while at $T = low$ and $T = T_{high}$ Ising model has a strikingly different degree distribution. We choose to display only one day's worth of kinetic energy measurements, yet we analyzed multiple days from different trials and acquired similar degree distributions for all of them. This data is presented in the Appendix A1.

Besides obvious visual similarities, several statistical characteristics are shared by the Ising model at the vicinity of the critical point and the Beehive and are notably absent when $T = T_{low}$ or $T = T_{High}$. As it is summarised in the table 1 the Ising model at $T = T_{crit}$ is best described by the power-law, while at low and high temperatures the best fit for the data is the Log-normal distributions. Different powerlaw exponents, as well as the different numbers of nodes explain the somewhat different shape of degree distribution for Ising model at $T = T_{crit}$ and the Beehive, however, general features of heavy-tailed distribution are evident in both cases.
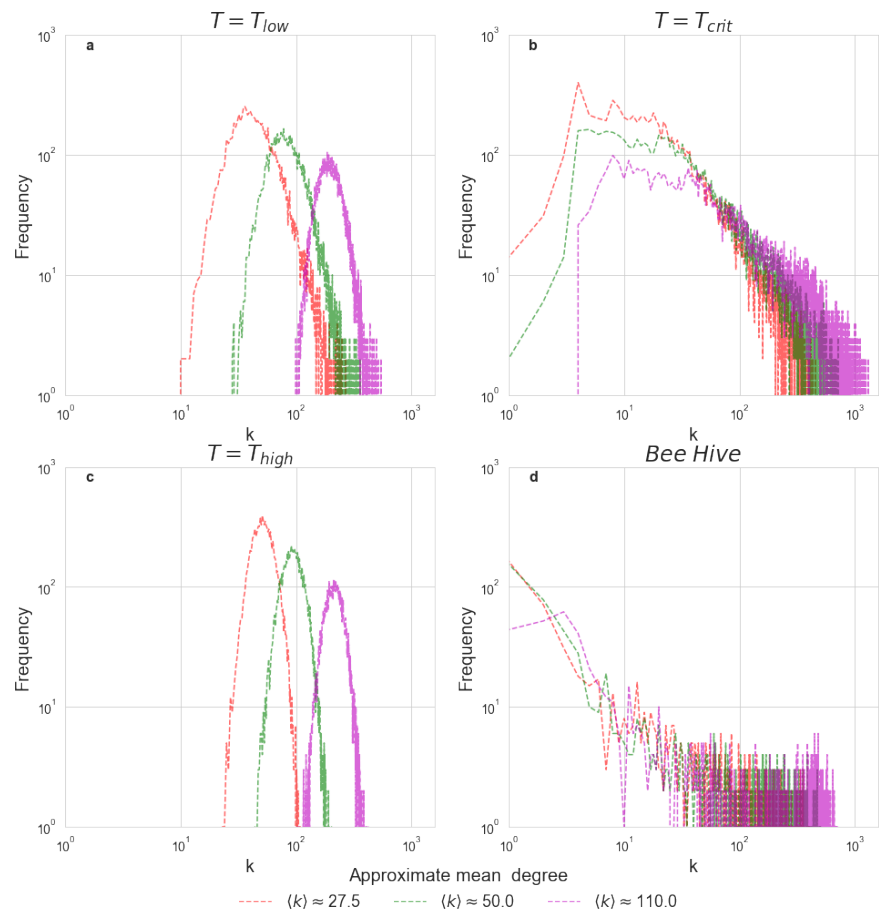
Figure 3. Degree distribution for the correlation networks. Panels (**a**), (**b**) and (**c**) depict the degree distributions of the Ising networks at T=2, T=2.3 and T=3. Panel (**d**) depicts an exemplifying degree distribution computed using bee hive activity during 1 day. For each network 3 representative values of $\langle k \rangle$ are plotted.

Table 1. Characteristics of Degree frequency distributions for various correlation networks. For Lognormal distribution mean μ and standard deviation σ are given. Truncated powerlaw distributions are characterized by the powerlaw exponent α and x_{min}. The latter specifies the minimum value of the data for which the powerlaw holds. All networks have matching mean degree $\langle k \rangle \approx 110$

System	Distribution family	Parameters of the distribution
Ising Model, $T = T_{low}$	*Lognormal*	$\mu = 4.12, \quad \sigma = 0.132$
Ising Model, $T = T_{crit}$	*Truncated Power-law*	$\alpha = 1.99, \quad x_{min} = 2$
Ising Model, $T = T_{high}$	*Lognormal*	$\mu = 3.58, \quad \sigma = 0.225$
Bee Hive	*Truncated Power-law*	$\alpha = 3.49, \quad x_{min} = 3$

3.2. Network metrics

Besides the degree distribution networks can be characterized by a number of other metrics, which account not only for the number of edges per node but also for the intertwined structure of the connections. Table 2 presents most common [36] metrics computed for the correlation networks of the Ising model and various beehives of similar mean degrees. Additional information about the metrics we used is given in the Appendix A.2

and supplementary tables describing the same networks tresholded at different mean degrees are available in A.2. In order to compute some characteristics, such as for example Average path length L it is necessary for the network to be fully connected. Bee correlation networks have a significant number of isolated nodes, although they always pertain a giant component of significant size, regardless of the threshold value. Ising model always remain fully connected at $T = T_{low}$ and $T = T_{high}$. Interestingly enough isolated subgraphs begin to appear in the network at $T = T_{crit}$ when threshold p is set to higher values.

We extract we giant component from the networks and use it to compute metrics. Thus $\langle k \rangle$ can vary within reasonable limits. Common technique in the study of networks is to compare the network at hand with a random graph. For each of the networks we created an ensemble of equivalent random Erdos-Renui graphs and computed their average characteristics as a reference.

Table 2. Network metrics computed for the giant components of correlation Graphs of Ising model and Bee hive. N-number of nodes, $\langle k \rangle$ - mean degree, C - average clustering coefficient, L - average path Length, D - diameter of the network. C_{rand}, L_{rand}, D_{rand} refer to the metrics computed on ensemble of Erdos-Renui graphs with N and $\langle k \rangle$ identical to the original network

	N	$\langle k \rangle$	C	L	D	C_{rand}	L_{rand}	D_{rand}
$T = T_{high}$	10000.0	111.51980	0.08664	2.04040	3.0	0.02237	1.98442	3.0
$T = T_{crit}$	10000.0	109.65700	0.55828	3.70079	14.0	0.02194	1.98597	3.0
$T = T_{low}$	10000.0	107.26360	0.08130	2.03172	3.0	0.02118	1.98836	3.0
Trial 5	1166.0	110.32333	0.63224	1.91577	4.0	0.18797	1.81092	2.0
Trial 4	1138.0	109.28559	0.50052	1.81285	3.0	0.19185	1.80776	2.0
Trial 3	1137.0	110.95163	0.52267	1.81035	3.0	0.19605	1.80486	2.0
Trial 2	1097.0	114.12306	0.71736	2.05477	7.0	0.20800	1.79177	2.0
Trial 1	946.0	111.74313	0.61843	1.80857	4.0	0.23652	1.76367	2.0

It can be noted, that correlation networks of the bee hive and of the Ising model at the critical temperature have much higher average clustering than both their random equivalents and correlation networks of Ising model at low and high temperatures. The average Path length in these clustered networks is generally somewhat higher than in the random networks, but considerably lower than if the graph had been a regular lattice with high clustering. Such graph structure, which combines high clustering characteristics of lattice-like networks with relatively low average path length, inherent to random graphs is known as the small-world network [37].

3.3. Temporal correlations

As it has been noted earlier, the critical state manifests itself not only in through spatial correlations, but also in the increased autocorrelations within the time-series. We computed the Hurst exponent H to elucidate presence of autocorrelations. High values H imply that the system which generated the timeseries at hand is in the vicinity of the critical state. Mean magnetization M time-series of the Ising model is characterized by a high value of H only when T is close to T_{crit} [33]. A common technique is to compare the time-series generated by the system of study with another time-series generated by a computational model which is known to exhibit critical behavior. For example [38] such technique was used to show that temporal patterns of blackouts in the USA exhibit characteristics of the critical state.

Figure 4 exhibits different Hurst exponents computed for the Ising model at different temperatures and exemplifying case of the Hurst exponent computed for the K_{mean} during a single day. H computed for other days shows only minor differences and H value is always significantly higher than 0.5. This is indicative of long-term corelations within the timeseries. As a sanity check we also computed H for randomly permuted mean kinetic energy time-series and as it would be expected of essentially random data $H \approx 0.5$. Ising model only displays high H values at $T = T_{crit}$, this finding as consistent both

with the previous research on the model and with the established connection between autocorrelations and criticality.
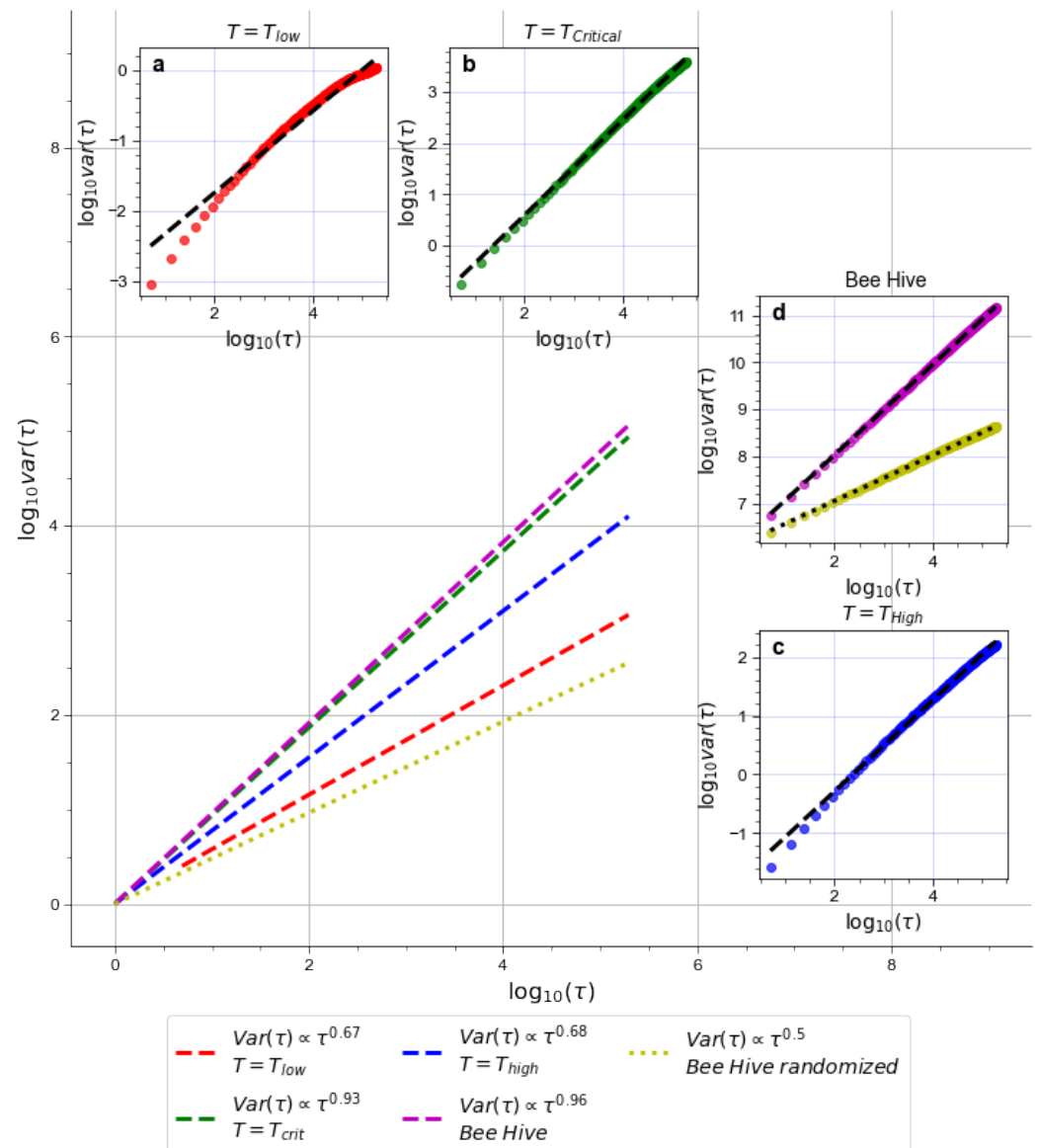
Figure 4. Hurst exponents for magnetization time-series of the Ising model and K_{mean} time-series of the bee hive. The main pane of the figure shows the slopes of the Hurst exponents for different timeseries in relation to each other. Inset panes (**a**), (**b**), (**c**) and (**d**) demonstrate how well H values fit the data.

4. Discussion

4.1. Summary of key findings

In our work, we analyzed a dataset of bee trajectories in a way that allowed us to compare our empirical data to a well-studied model. Such an approach has been previously used [16] to show that key dynamical characteristics of the human brain at its resting state bear significant resemblance to the Ising model when the latter is in the vicinity of the critical state. With some minor differences, which are to be expected, given the different nature of the data, our analysis of bee correlation networks yielded remarkably similar results - similarity between the Ising model and $T = T_{crit}$ and lack of thereof at low and high temperatures. Furthermore, structural analysis of correlation networks showed that certain characteristics, most notably clustering and path length are compatible between

the network of bee correlations and critical state of the model and are drastically different otherwise. Analysis of mean parameters K_{mean} and M showed that recordings of the average activity of both the Bee Hive and the Ising model at the critical state are marked with considerable autocorrelations within the time-series.

Earlier research [16] showed, that correlation networks of the Ising model bear similarity to the resting state neural dynamics only at the critical state. Long-range temporal autocorrelations are also considered to be a hallmark of criticality both in the Ising model and in the neural timeseries [39].

4.2. Critical brains and critical swarms

We believe that our results provide considerable evidence in support of what we would call a "critical swarm" hypothesis. As we had summarised earlier 1.2 critical state benefits the cognitive ability, to an extend that in can be argued that such state is not simply advantageous, but necessary. At the same time, convincing arguments 1.1 imply that social insects are endowed with a sort of collective cognitive capacity, which, despite the entirely different modes of organization, shares some key similarities with the mammalian brains. Thus, we believe that the benefits critical state brings, would be desirable for both these systems.

Previous research showed that some of the hallmarks of critical state are observable in swarming midges [24] and flocking birds [23]. Moreover, previous research on the same dataset [28] found that time-series of the K_{mean} of the beehive incorporate bursts of activity, significantly exceeding the average level, which are interspersed with quiescent periods. The distribution of waiting times between these burst abides by the power-law distribution. This was also found to be the case for "avalanches" in Back-Wisenfield sandpile, a famous model of self-organized criticality [40], and for the patterns of the Neural activity recorded in the cortical slices of mice [15] *in vitro*.

One of the benefits of the critical state in the neural networks is that it enables easier integration of information. Our findings show that correlation graphs of bee activity exhibit distinct small-world structure 3.2 and that this organization also emerges in the Ising Model when $T = T_{crit}$. Such network structure is known to enhcnace systems' capacity to integrate information. One should note, that in the human brain small-world architecture of functional connectivity is undergrid by a similar structural organization of cortical connectivity [41,42]. Bee hive and the critical Ising model have drastically different underlying structures, one being the regular lattice, other having no connectivity constraints. Yet, their functional connectivity is remarkably similar. Uncovering small-world structure in the functional correlation of the bees might signify, that this type of organisation, ubiquitous in the brain, is even more fundamental to the functionality of any cognitive system than it was previously considered.

Other notable features of the network structure, shared by both the critical Ising model and the bee hive data, is the presence of hubs - nodes with exceptionally high degree. And again it is important to observe that such features arose in the dynamics of the system without any preexisting structural frameworks which might have channeled the activity.

We should highlight several important differences between our work and the corpus of research that concerns hallmarks of criticality in the swarm dynamics, as well as with the studies employing tools of network science to study eusocial insects [2,43]. The most notable dissimilarity with the latter is that most studies we reviewed focused on social networks, constructed by observing species-specific means of communication, such as trophallaxis in bees and attenuation in ants. Such contacts, important as they are, only constitute a minuscule amount of individuals' insect total activity and, as we believe, account only for a portion of total informational exchange that takes place inside the hive. Significant correlations between kinetic energy time-series and highly specific degree distributions of the correlation graph, in our view, reflect some features of underlying computation in the hive, aided by its critical state.

Hallmarks of critical behavior, when studied previously, were investigated in freely-moving agents: flocking birds or swarming midges. Thus, it is possible to argue, that observed features, such as the long-range velocity correlations, were begotten by the spatial order the organisms maintained. Indeed, most critical phenomena nature abounds with are exhibited by systems that possess no cognitive ability, collective or otherwise.

Data we analyzed was acquired when bees were locked inside the hive and provided with sustenance. They were under no pressure to maintain a specific movement order, as they would have been during swarming, or to move at all, in fact. Thus, we believe that, given the conditions, the hallmarks of the critical state we analyzed would be observed only if such state is inherent to the system, much like it is to the human brain at its resting state.

5. Conclusions

Our findings strongly imply that the honey bee swarm is a critical system. However, complexity of the issue dictates that further work is required to ascertain the conjecture that colonies of eusocial insects are critical. It is crucial to analyze other datasets, to confirm that hallmarks of the kind we observed are ubiquitous across bee spices and to analyze other eucsocial insects, such as ants and termites. Moreover, criticality manifests itself on different levels - we focused on temporal and spatial correlations, however other aspects, for example, behavior of the system during the coarse-graining should also be considered. Other vantage direction is to explore how the critical state is affected by the hives' normal activity, such as foraging and swarming, as well as by the environmental factors, such as the day-night cycle.

Comparing high-level descriptions of different systems could shed light on patterns that are imperceptible when the focus is too narrow. Thus, much ink had been spilled by some of the best scientific minds in debating the validity of the critical brain hypothesis and the debate is still not settled [44]. Evidence from other fields could tip the scales in the ongoing discussion.

Author Contributions: All authors have read and agreed to the published version of the manuscript.

Funding: This research received no external funding.

Data Availability Statement: Data for this study was provided by the third party.

Acknowledgments: We thank professor Gene Robinson and his team for sharing the dataset used in our research

Conflicts of Interest: The Authors declare no conflict of interest

Abbreviations

The following abbreviations are used in this manuscript:

FMRI	Functional magnetic resonance imaging
EEG	An electroencephalogram
LFP	Local field potentials

Appendix A. Algorithms and metrics

Appendix A.1. Monte-Carlo Algorithm

Metropolis Monte-Carlo Algorithm is commonly used to computationally solve for the equilibrium configuration of the Ising model. This approach assumes that the system is submerged in the heat bath of temperature T. Steps of the algorithm are summarized below.

1. Initialise the model with random configuration of spins
2. Select random site and flip its spin

3. Compute the energy of the new configuration using (4), than compute energy difference with the previous configuration $\delta E = E_{new} - E_{old}$.

4. If $\delta E \leq 0$ accept the change.

5. Else, if $\delta E > 0$

  i   Compute transition probability $w = e^{\frac{\delta E}{kT}}$

  ii   Generate a random number r in the unit interval

  iii Accept the change if $r \leq w$

6. Return to step 1

Appendix A.2. Network Metrics

To concisely characterise network topology several common metrics are used [36]. Clustering quantifies the propensity of nodes in the network to cluster together i. e how likely is that neighbours of a node would also be connected amongst each other. For a graph G described by an adjacency matrix A local clustering coefficient C_i can be computed using equation (A1) and average clustering C is simply the mean (A2) of the local clustering coefficients for each node of the network.

$$C_i = \frac{1}{k_i(k_i - 1)} \sum_{j,k} A_{ij} A_{jk} A_{ki} \tag{A1}$$

$$k_i - degree\ of\ a\ node$$

$$C = \frac{1}{n} \sum_{i=1}^{n} C_i \tag{A2}$$

Average path length is the mean number of steps required to traverse from one node to another. If shortest distance between any two nodes, v_i and v_j is defined as $d(v_i, v_j)$, then average distance for all possible pairs on nodes in the networks could be computed using (A3).

$$L = \frac{1}{n(n-1)} \sum_{i \neq j} d(v_i, v_j) \tag{A3}$$

In our work we computed all possible shortest paths using Dijkstra's algorithm and than found an average L for the whole network. Final metric we used is the diameter of the network D - which is equal to longest possible shortest path.

Appendix B. Supplementary Data

Appendix B.1. Supplementary Graphs
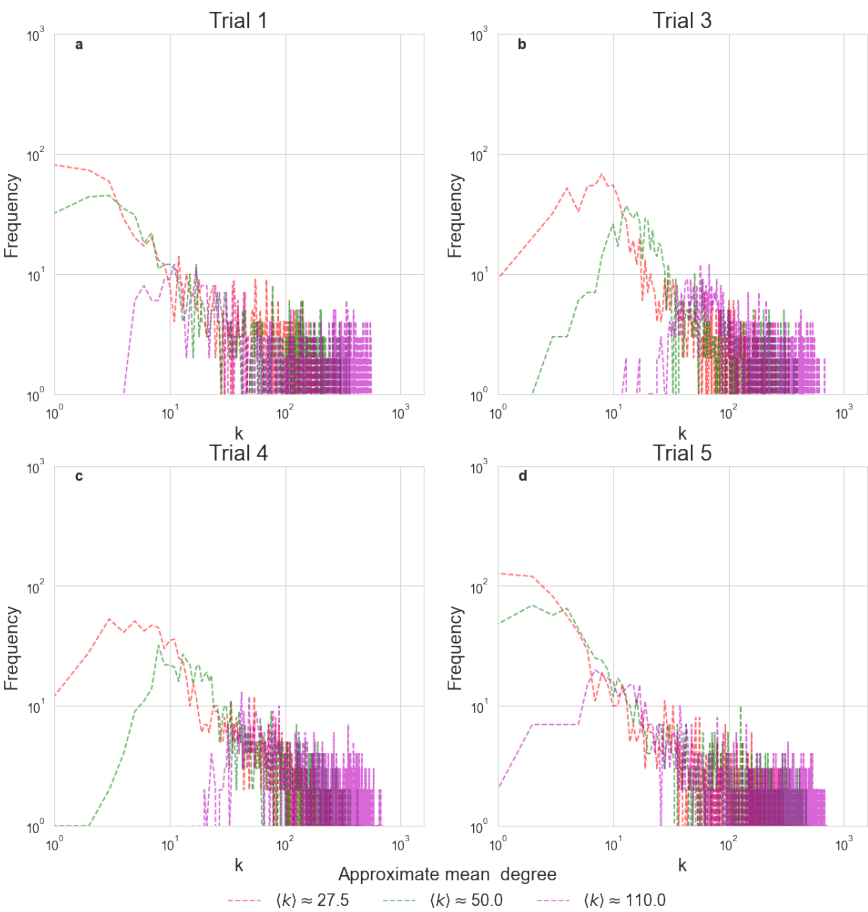
Figure A1. Degree distribution for correlation networks. Panel (**a**), (**b**), (**c**) and (**d**) depict different Trials using different hives. Methods used to generate depicted degree distributions are identical to those used to produce Figure 3
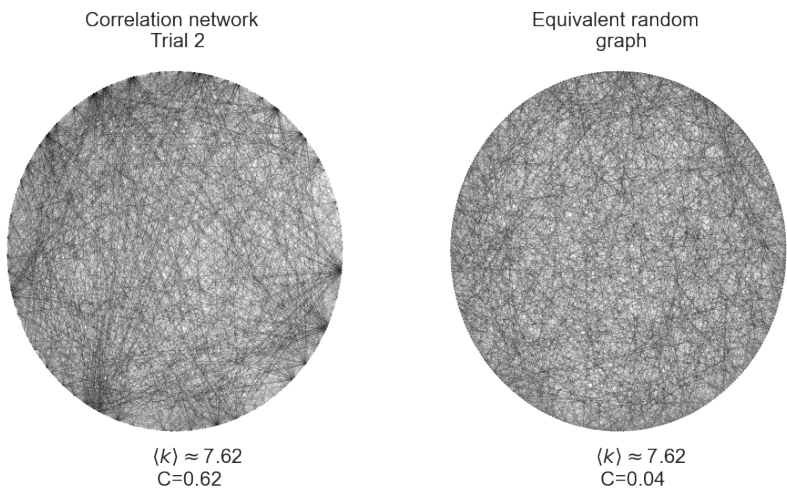
Figure A2. Illustrative images depicting of the bee correlation network and equivalent random network. Mean degrees $\langle k \rangle$ and average clustering coefficients C are given below each image pane. Low mean degrees and thus sufficiently high threshold values have been used for clarity of visualisation.

Appendix B.2. Log-likelihood tables

Fitting a power-law to an empirical distribution is a task that requires due caution. The most rigorous approach developed requires comparing hypothetical power-law fit with other candidate long-tailed distributions [30]. Most important of them is the exponential distribution, however log-normal and stretched exponential (Weibull) should also be considered. Furthermore, using different thresholds to binarise the correlation matrices could also affect the characteristics of resultant degree distribution. Thus, to provide a comprehensive view of our analysis below we present the table of log-likelihood tests for different dataset used in our work.

Log-likelihood tables A1, A2, A3 and A4 summarise results of statistical tests for different systems thresholded at various mean degrees. Each case is tested against 3 candidate distributions: Exponential, Log-normal and Weibull. Possible lognormal distributions are restricted to those with positive mean *mu*, for otherwise, one would have to assume possibility of node having negative degree. For each test two values are generated: log-likelihood ℓ and p-value p. $\ell > 0$ implies that power-law distribution is preferred, $\ell < 0$ signifies that another candidate distribution provides a better fit to the data. p indicates the statistical significance of the uncovered relationship. Careful examination of the provided summary tables allows to conclude, that although in some cases Ising model at $T = T_{low}$ could exhibit power-law relationship, in overwhelming majority of cases such relationship exists only in the vicinity of the critical point of the Ising model. Similar summary judgement illuminates presence of clear power-law scaling in the degree distribution of bee correlations.

Table A3. Log-likelihood ratios with their respective p-values computed for degree distributions of correlation networks of the different Bee Hives during different trials. Part 1.

Model	Mean Degree Log-likelihood, p-value Distribution	$\langle k \rangle \approx 60.0$		$\langle k \rangle \approx 90.0$		$\langle k \rangle \approx 110.0$	
		ℓ	p	ℓ	p	ℓ	p
Trial 1	Exponential	35.2344	0.0057	11.1576	0.0029	2.6810	0.1226
	Log-normal	1.9488	0.5026	1.8850	0.1182	0.5636	0.0446
	Weibull	-0.0331	0.9416	0.2664	0.3008	0.2525	0.0030
Trial 3	Exponential	26.0145	0.0000	3.3355	0.0999	0.0021	0.9967
	Log-normal	1.7951	0.1321	1.3102	0.0007	0.4929	0.0104
	Weibull	0.7285	0.0249	0.6027	0.0002	-0.0046	0.9910
Trial 4	Exponential	12.8372	0.0037	-0.0114	0.4864	0.2154	0.7090
	Log-normal	1.2979	0.1088	-0.1651	0.7009	0.2560	0.0932
	Weibull	0.4883	0.0046	-0.2188	0.6598	0.0524	0.5102
Trial 5	Exponential	72.9602	0.0000	43.4732	0.0001	11.1195	0.0029
	Log-normal	9.4708	0.0086	4.8933	0.1093	1.6425	0.0999
	Weibull	0.9996	0.1582	0.3480	0.3929	0.3398	0.0002

Table A1. Log-likelihood ratios with their respective p-values computed for degree distributions of correlation networks of the Bee hive and the Ising model tresholded at different mean degrees. Part 1.

Model	Mean Degree Log-likelihood, p-value Distribution	$\langle k \rangle \approx 20.0$		$\langle k \rangle \approx 27.5$		$\langle k \rangle \approx 50.0$	
		ℓ	p	ℓ	p	ℓ	p
$T = T_{low}$	Exponential	14.0710	0.0224	9.7538	0.1672	-0.1100	0.0539
	Log-normal	5.5999	0.0000	5.0950	0.0185	-1.6257	0.3173
	Weibull	1.9843	0.1524	-0.3715	0.8911	-1.7395	0.2904
$T = T_{crit}$	Exponential	160.9710	0.0000	269.4061	0.0000	296.9442	0.0000
	Log-normal	7.7403	0.0000	10.8814	0.0000	14.2553	0.0000
	Weibull	4.2434	0.0000	4.9645	0.0000	6.5738	0.0000
$T = T_{high}$	Exponential	-3.4572	0.5225	7.9102	0.4883	-0.1400	0.0288
	Log-normal	0.5453	0.8520	0.5159	0.8926	-2.5385	0.1892
	Weibull	-4.2745	0.2793	-7.1229	0.1479	-3.1692	0.1353
Bee Hive	Exponential	68.3686	0.0040	109.4801	0.0061	118.1101	0.0035
	Log-normal	5.5905	0.0696	8.0556	0.1236	10.2539	0.1191
	Weibull	1.1172	0.1596	1.3214	0.2896	1.8727	0.1386

Table A2. Log-likelihood ratios with their respective p-values computed for degree distributions of correlation networks of the Bee hive and the Ising model tresholded at different mean degrees. Part 2.

Model	Mean Degree Log-likelihood, p-value Distribution	$\langle k \rangle \approx 60.0$		$\langle k \rangle \approx 90.0$		$\langle k \rangle \approx 110.0$	
		ℓ	p	ℓ	p	ℓ	p
$T = T_{low}$	Exponential	-0.1507	0.0336	-0.2025	0.0005	-0.6169	0.0000
	Log-normal	-1.9751	0.2443	-5.3950	0.0348	-9.5480	0.0161
	Weibull	-2.2142	0.1969	-5.8917	0.0221	-10.4566	0.0152
$T = T_{crit}$	Exponential	335.6884	0.0000	353.2331	0.0000	330.8069	0.0000
	Log-normal	18.0843	0.0000	20.5435	0.0000	20.3117	0.0000
	Weibull	6.7255	0.0000	7.7506	0.0000	8.8427	0.0000
$T = T_{high}$	Exponential	-0.1408	0.0057	-27.3007	0.0000	-0.2165	0.0316
	Log-normal	-3.9967	0.0747	-13.9405	0.0325	-2.0616	0.2600
	Weibull	-4.7758	0.0521	-29.7762	0.0002	-2.9617	0.1781
Bee Hive	Exponential	114.6828	0.0014	92.1413	0.0017	79.2483	0.0006
	Log-normal	13.1142	0.0297	11.4028	0.0448	11.5063	0.0243
	Weibull	2.2617	0.0898	1.6717	0.1223	1.7065	0.0941

Table A4. Log-likelihood ratios with their respective p-values computed for degree distributions of correlation networks of the different Bee Hives during different trials. Part 2.

Model	Mean Degree Log-likelihood, p-value Distribution	$\langle k \rangle \approx 20.0$ ℓ	p	$\langle k \rangle \approx 27.5$ ℓ	p	$\langle k \rangle \approx 50.0$ ℓ	p
Trial 1	Exponential	42.0251	0.0122	39.4696	0.0006	37.1392	0.0000
	Log-normal	-0.5323	0.7987	3.6085	0.1000	6.6321	0.0018
	Weibull	-0.5369	0.4757	0.6376	0.2998	1.2888	0.0250
Trial 3	Exponential	51.6177	0.0000	47.7674	0.0000	23.9114	0.0000
	Log-normal	2.2136	0.2228	1.8331	0.3150	2.6847	0.0234
	Weibull	0.4194	0.1938	0.3688	0.3130	0.6090	0.0022
Trial 4	Exponential	16.3384	0.0003	17.4676	0.0000	12.4347	0.0018
	Log-normal	0.6153	0.3228	1.1261	0.1393	0.7740	0.1541
	Weibull	0.3341	0.1844	0.3577	0.0760	0.4721	0.0631
Trial 5	Exponential	58.6767	0.0000	76.2392	0.0001	80.6464	0.0000
	Log-normal	5.7597	0.0110	4.8574	0.1337	9.6371	0.0113
	Weibull	1.2528	0.0668	0.4872	0.4708	1.1838	0.1514

Appendix B.3. Networks Metrics

In this section we provide some supplementary information on networks metrics. Methods are identical to those used in 3.2, however different combination of mean degrees and tresholds was used.

Table A5. Supplementary table on network metrics, part 1

	N	$\langle k \rangle$	C	L	D	C_{rand}	L_{rand}	D_{rand}
$T = T_{low}$	10000.0	27.77980	0.10345	2.79937	4.0	0.00552	2.72503	4.0
$T = T_{high}$	10000.0	27.33960	0.22436	2.86948	4.0	0.00566	2.73211	4.0
$T = T_{crit}$	9990.0	27.56977	0.52762	7.71826	31.0	0.00571	2.72821	4.0
Trial 4	1135.0	27.06872	0.33549	2.44105	5.0	0.04775	2.02390	3.0
Trial 3	1135.0	26.84141	0.32411	2.49355	5.0	0.04734	2.02858	3.0
Trial 5	1066.0	29.88555	0.49939	2.74393	7.0	0.05540	1.97709	3.0
Trial 1	879.0	29.36177	0.41123	2.54526	8.0	0.06622	1.95331	3.0
Trial 2	783.0	39.68199	0.67767	2.52859	12.0	0.10136	1.89870	3.0

Table A6. Supplementary table of network metrics, part 2

	N	$\langle k \rangle$	C	L	D	C_{rand}	L_{rand}	D_{rand}
$T = T_{crit}$	10000.0	50.16580	0.55841	5.44477	20.0	0.01022	2.35186	3.0
$T = T_{low}$	10000.0	48.71740	0.08564	2.50541	4.0	0.00942	2.37342	3.0
$T = T_{high}$	10000.0	49.54980	0.12720	2.53886	4.0	0.00945	2.36108	3.0
Trial 5	1138.0	52.04218	0.52962	2.36404	6.0	0.09158	1.90867	3.0
Trial 4	1138.0	48.77768	0.39881	2.10649	4.0	0.08457	1.91453	3.0
Trial 3	1137.0	48.68338	0.41045	2.13271	4.0	0.08617	1.91448	3.0
Trial 2	934.0	60.53426	0.66733	2.43440	9.0	0.12875	1.87055	2.0
Trial 1	933.0	51.37835	0.48489	2.22992	7.0	0.11022	1.88991	3.0

References

1. Couzin, I.D. Collective cognition in animal groups. *Trends in cognitive sciences* **2009**, *13*, 36–43.
2. Gernat, T.; Rao, V.D.; Middendorf, M.; Dankowicz, H.; Goldenfeld, N.; Robinson, G.E. Automated monitoring of behavior reveals bursty interaction patterns and rapid spreading dynamics in honeybee social networks. *Proceedings of the National Academy of Sciences* **2018**, *115*, 1433–1438.
3. Detrain, C.; Deneubourg, J.L. Self-organized structures in a superorganism: do ants "behave" like molecules? *Physics of life Reviews* **2006**, *3*, 162–187.
4. Peleg, O.; Peters, J.M.; Salcedo, M.K.; Mahadevan, L. Collective mechanical adaptation of honeybee swarms. *Nature Physics* **2018**, *14*, 1193–1198.

5. Mlot, N.J.; Tovey, C.A.; Hu, D.L. Fire ants self-assemble into waterproof rafts to survive floods. *Proceedings of the National Academy of Sciences* **2011**, *108*, 7669–7673.

6. Seeley, T.D. Honeybee democracy. In *Honeybee Democracy*; Princeton University Press, 2010.

7. Gelblum, A.; Fonio, E.; Rodeh, Y.; Korman, A.; Feinerman, O. Ant collective cognition allows for efficient navigation through disordered environments. *ELife* **2020**, *9*, e55195.

8. Marting, P.R.; Wcislo, W.T.; Pratt, S.C. Colony personality and plant health in the Azteca-Cecropia mutualism. *Behavioral ecology* **2018**, *29*, 264–271.

9. Reina, A.; Bose, T.; Trianni, V.; Marshall, J.A. Psychophysical laws and the superorganism. *Scientific reports* **2018**, *8*, 1–8.

10. Chialvo, D.R. Emergent complex neural dynamics. *Nature physics* **2010**, *6*, 744–750.

11. Schnell, A.K.; Amodio, P.; Boeckle, M.; Clayton, N.S. How intelligent is a cephalopod? Lessons from comparative cognition. *Biological Reviews* **2021**, *96*, 162–178.

12. Hesse, J.; Gross, T. Self-organized criticality as a fundamental property of neural systems. *Frontiers in systems neuroscience* **2014**, *8*, 166.

13. Bak, P. *How nature works: the science of self-organized criticality*; Springer Science & Business Media, 2013.

14. Sethna, J. *Statistical mechanics: entropy, order parameters, and complexity*; Vol. 14, Oxford University Press, USA, 2021.

15. Beggs, J.M.; Plenz, D. Neuronal avalanches in neocortical circuits. *Journal of neuroscience* **2003**, *23*, 11167–11177.

16. Fraiman, D.; Balenzuela, P.; Foss, J.; Chialvo, D.R. Ising-like dynamics in large-scale functional brain networks. *Physical Review E* **2009**, *79*, 061922.

17. Kitzbichler, M.G.; Smith, M.L.; Christensen, S.R.; Bullmore, E. Broadband criticality of human brain network synchronization. *PLoS computational biology* **2009**, *5*, e1000314.

18. Schuster, H.G. *Criticality in neural systems*; John Wiley & Sons, 2014.

19. Shew, W.L.; Yang, H.; Yu, S.; Roy, R.; Plenz, D. Information capacity and transmission are maximized in balanced cortical networks with neuronal avalanches. *Journal of neuroscience* **2011**, *31*, 55–63.

20. Shriki, O.; Yellin, D. Optimal information representation and criticality in an adaptive sensory recurrent neuronal network. *PLoS computational biology* **2016**, *12*, e1004698.

21. Shew, W.L.; Yang, H.; Petermann, T.; Roy, R.; Plenz, D. Neuronal avalanches imply maximum dynamic range in cortical networks at criticality. *Journal of neuroscience* **2009**, *29*, 15595–15600.

22. Zimmern, V. Why brain criticality is clinically relevant: a scoping review. *Frontiers in neural circuits* **2020**, *14*, 54.

23. Cavagna, A.; Queirós, S.D.; Giardina, I.; Stefanini, F.; Viale, M. Diffusion of individual birds in starling flocks. *Proceedings of the Royal Society B: Biological Sciences* **2013**, *280*, 20122484.

24. Attanasi, A.; Cavagna, A.; Del Castello, L.; Giardina, I.; Melillo, S.; Parisi, L.; Pohl, O.; Rossaro, B.; Shen, E.; Silvestri, E.; et al. Collective behaviour without collective order in wild swarms of midges. *PLoS computational biology* **2014**, *10*, e1003697.

25. Attanasi, A.; Cavagna, A.; Del Castello, L.; Giardina, I.; Melillo, S.; Parisi, L.; Pohl, O.; Rossaro, B.; Shen, E.; Silvestri, E.; et al. Finite-size scaling as a way to probe near-criticality in natural swarms. *Physical review letters* **2014**, *113*, 238102.

26. Gelblum, A.; Pinkoviezky, I.; Fonio, E.; Ghosh, A.; Gov, N.; Feinerman, O. Ant groups optimally amplify the effect of transiently informed individuals. *Nature communications* **2015**, *6*, 1–9.

27. Li, L.; Peng, H.; Kurths, J.; Yang, Y.; Schellnhuber, H.J. Chaos–order transition in foraging behavior of ants. *Proceedings of the National Academy of Sciences* **2014**, *111*, 8392–8397.

28. Doi, I.; Ikegami, T. Endogenous and exogenous bursts in a honey bee hive. In Proceedings of the Artificial Life Conference Proceedings. MIT Press One Rogers Street, Cambridge, MA 02142-1209, USA journals-info . . . , 2018, pp. 493–499.

29. Gould, H.; Tobochnik, J. *Computer simulation methods*; Addison-Wesley Reading, 1996.

30. Clauset, A.; Shalizi, C.R.; Newman, M.E. Power-law distributions in empirical data. *SIAM review* **2009**, *51*, 661–703.

31. Alstott, J.; Bullmore, E.; Plenz, D. powerlaw: a Python package for analysis of heavy-tailed distributions. *PloS one* **2014**, *9*, e85777.

32. Fraiman, D.; Chialvo, D.R. What kind of noise is brain noise: anomalous scaling behavior of the resting brain activity fluctuations. *Frontiers in physiology* **2012**, *3*, 307.

33. Zhao, L.; Li, W.; Yang, C.; Han, J.; Su, Z.; Zou, Y. Multifractality and network analysis of phase transition. *PloS one* **2017**, *12*, e0170467.

34. Mandelbrot, B.B.; Wallis, J.R. Noah, Joseph, and operational hydrology. *Water resources research* **1968**, *4*, 909–918.

35. Stan, C.; Cristescu, C.M.; Cristescu, C.P. Computation of hurst exponent of time series using delayed (log-) returns. Application to estimating the financial volatility. *University Politechnica of Bucharest Scientific Bulletin* **2014**, *76*, 235–244.

36. Newman, M. *Networks*; Oxford university press, 2018.

37. Watts, D.J.; Strogatz, S.H. Collective dynamics of 'small-world' networks. *nature* **1998**, *393*, 440–442.

38. Carreras, B.A.; Newman, D.E.; Dobson, I.; Poole, A.B. Evidence for self-organized criticality in a time series of electric power system blackouts. *IEEE Transactions on Circuits and Systems I: Regular Papers* **2004**, *51*, 1733–1740.

39. Meisel, C.; Bailey, K.; Achermann, P.; Plenz, D. Decline of long-range temporal correlations in the human brain during sustained wakefulness. *Scientific reports* **2017**, *7*, 1–11.

40. Bak, P.; Tang, C.; Wiesenfeld, K. Self-organized criticality: An explanation of the $1/f$ noise. *Physical review letters* **1987**, *59*, 381.

41. Liao, X.; Vasilakos, A.V.; He, Y. Small-world human brain networks: perspectives and challenges. *Neuroscience & Biobehavioral Reviews* **2017**, *77*, 286–300.

42. Sporns, O. *Networks of the Brain*; MIT press, 2016.

43. Waters, J.S.; Fewell, J.H. Information processing in social insect networks. *PloS one* **2012**, *7*, e40337.

44. Beggs, J.M.; Timme, N. Being critical of criticality in the brain. *Frontiers in physiology* **2012**, *3*, 163.